SHADOW AND SPECULAR REMOVAL BY PHOTOMETRIC LINEARIZATION BASED ON PCA WITH OUTLIER EXCLUSION

Takahiro Mori[1], Shinsaku Hiura[2] and Kosuke Sato[1]

[1]*Graduate School of Engineering Sciences, Osaka University, 1-3 Machikaneyama, Toyonaka, 560-8531 Osaka, Japan*

[2]*Graduate School of Information Sciences, Hiroshima City University, 3-4-1 Ozukahigashi, Asaminamiku, 731-3194 Hiroshima, Japan*

Keywords: Photometric Linearization, Reflection Components, Shadow Removal.

Abstract: The photometric linearization method converts real images, including various photometric components such as diffuse reflection, specular reflection, attached and cast shadow, into images with diffuse reflection components only, which satisfies the Lambertian law. The conventional method(Mukaigawa et al., 2007) based on a random sampling framework successfully achieves the task; however, it contains two problems. The first is that the three basis images selected from the input images by the user seriously affect the linearization result quality. The other is that it takes a long time to process the enormous number of random samples needed to find the correct answer probabilistically. We therefore propose a novel algorithm using the PCA (principal component analysis) method with outlier exclusion. We used knowledge of photometric phenomena for the outlier detection and the experiments show that the method provides fast and precise linearization results.

1 INTRODUCTION

Most photometric analysis methods assume that the input images follow the Lambertian law. It is therefore important to generate images with only diffuse reflections from the input images with other photometric components, such as specular reflections and shadows.

Several methods have already been proposed for separation of photometric components. The dichromatic reflection model(Shafer, 1985) is often used(Klinker et al., 1988; Sato and Ikeuchi, 1994; Sato et al., 1997) for the separation. If the colors of the objects are quite different from the color of the light source, the model is very effective. However, if the two colors are similar, the separation becomes unstable. This method is of course not applicable for monochromatic images.

The polarization is also useful for the separation process. Wolff and Boult(Wolff and Boult, 1991) proposed a method to separate specular reflections by analyzing the reflected polarization, while Nayar et al.(Nayar et al., 1993) used combined color and polarization clues to separate the specular reflections. These methods, however, have a common restriction in that they cannot handle shadows. The geometry of the scene is useful for the analysis of specular reflections and shadows. Ikeuchi and Sato(Ikeuchi and Sato, 1991) proposed a method to classify photometric components based on the range and brightness of the images. A shadowed area can be distinguished using the shape of the object, but it is not easy to measure the shape of the scene even in the occluded areas.

However, there are some methods that use the characteristics of diffuse reflection, which lies in a linear subspace. Shashua(Shashua, 1992) showed that an image illuminated from any lighting direction can be expressed by a linear combination of three basis images taken from different lighting directions, and assuming a Lambertian surface and a parallel ray. This means that an image can be perfectly expressed in a 3D subspace. Belhumeur and Kriegman(Belhumeur and Kriegman, 1996) showed that an image can be expressed using the illumination cone model, even if the image includes attached shadows. In the illumination cone, the images are expressed by using a linear combination of extreme rays. Georghiades et al.(Georghiades et al., 2001) extended the illumination cone model so that cast shadows can also be expressed using shape reconstruction. Although any photometric components can ideally be expressed using the illumination cone, large numbers of images corresponding to the extreme rays are necessary.

Based on Shashua's framework, Mukaigawa et

Mori T., Hiura S. and Sato K..
SHADOW AND SPECULAR REMOVAL BY PHOTOMETRIC LINEARIZATION BASED ON PCA WITH OUTLIER EXCLUSION.
DOI: 10.5220/0003817202210229
In *Proceedings of the International Conference on Computer Vision Theory and Applications* (VISAPP-2012), pages 221-229
ISBN: 978-989-8565-03-7

al.(Mukaigawa et al., 2007; Mukaigawa et al., 2001) proposed a method to convert real images into linear images with diffuse components using only the random sample consensus algorithm. The method can also classify each pixel into diffuse, specular, attached shadow and cast shadow areas. However, because their method starts from three manually selected input images, the result depends heavily on the image selection. Their algorithm also takes a very long time to find an adequate combination of diffuse pixels from an enormous set of random samples. Therefore, in this paper, we propose a novel algorithm using the PCA (principal component analysis) method with outlier exclusion. This method automatically generates basis images, and the deterministic algorithm guarantees much a shorter execution time. The outliers are distinguished by using the knowledge of photometric phenomena, and the results show that out algorithm provides better results than those using RANSAC-based outlier exclusion.

2 CLASSIFYING REFLECTION USING PHOTOMETRIC LINEARIZATION

From the viewpoint of illumination and reflection phenomena, each pixel on the input image is classified into several areas, as shown in Fig.1. According to the dichromatic reflection model(Shafer, 1985) shown in Fig.2, reflection consists of diffuse and specular reflections. While the observed intensity caused by diffuse reflection is independent of the viewing direction, specular reflection is only observed from a narrow range close to the mirror direction of the incident light. Shadows are also classified into attached shadows and cast shadows(Shashua, 1992). If the angle between the surface normal and the light direction is larger than a right angle, the intensity of the surface is zero and is called attached shadow. If there is an object between the light source and the surface, the incoming light is occluded by the object. This is called cast shadow.

In the following, we discuss the reflection phenomena using a linear model of diffuse reflection.

2.1 Classification of Reflections

The Lambertian model is a most basic reflection model of a matte surface, such as plaster. The intensity of the surface is represented as

$$i = \mathbf{n} \cdot \mathbf{s} \tag{1}$$

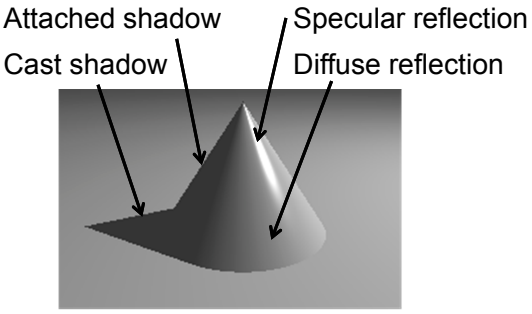

Figure 1: Illumination and reflection phenomena.

Figure 2: Dichromatic reflection model.

where $\mathbf{n}$ denotes the surface property vector, which is a product of a unit normal vector and the diffuse reflectance. Similarly, $\mathbf{s}$ represents the lighting property vector, which is a product of a unit vector towards the lighting direction and the brightness of the light.

In Eq.(1), if the angle between $\mathbf{n}$ and $\mathbf{s}$ is greater than 90°, the intensity i becomes negative, but, of course, there cannot be a negative power of light. In this case, the area on the object is observed as being attached shadow, and the intensity becomes zero instead of the negative value. To deal with the attached shadows as well as the diffuse reflections, the following equation is commonly used(Belhumeur and Kriegman, 1996).

$$i = max(\mathbf{n} \cdot \mathbf{s}, 0) \tag{2}$$

In contrast, as shown in Fig. 1, the angle between $\mathbf{n}$ and $\mathbf{s}$ is smaller than 90° in the area of a cast shadow. If there is no inter-reflection, the intensities of both shadowed areas are zero, and we can distinguish between the two shadow phenomena by using the sign of $\mathbf{n} \cdot \mathbf{s}$ if we know the surface normal and the lighting direction.

As shown in Fig. 2, the intensity of the specular reflection is an additional component to the diffuse reflection. Therefore, the intensity at the specular reflection is always greater than the value calculated with the Lambertian model. To summarize, we can distinguish the illumination and reflection components using the following chart.

$$\begin{cases} \text{Diffuse} & i = \mathbf{n} \cdot \mathbf{s} \\ \text{Specular} & i > \mathbf{n} \cdot \mathbf{s} \\ \text{Attached shadow} & i = 0 \cap \mathbf{n} \cdot \mathbf{s} \leq 0 \\ \text{Cast shadow} & i = 0 \cap \mathbf{n} \cdot \mathbf{s} > 0 \end{cases} \tag{3}$$

2.2 Photometric Linearization

Shashua(Shashua, 1992) showed that if a parallel ray is assumed, an image with N pixels $I_k = \begin{pmatrix} i_{(k,1)} & i_{(k,2)} & \cdots & i_{(k,N)} \end{pmatrix}^T$ of a diffuse object under any lighting direction can be expressed using a linear combination of three basis images, $(\hat{I}_1, \hat{I}_2, \textit{and } \hat{I}_3)$ taken using different lighting directions;

$$I_k = c_k^1 \hat{I}_1 + c_k^2 \hat{I}_2 + c_k^3 \hat{I}_3 \tag{4}$$

Here, let $C_k = \begin{pmatrix} c_k^1 & c_k^2 & c_k^3 \end{pmatrix}^T$ be a set of coefficients of the image I_k.

However, real images do not always satisfy Eq.(4), because specular reflections and shadows are commonly observed. Therefore, in this paper, we discuss the conversion of real images into linear images which include diffuse reflection components only. This conversion process is called photometric linearization and the converted images are called linearized images. Because linearized images should satisfy Eq.(4), all M input images could be expressed by using linear combination of the three basis images(Shashua, 1992) as

$$\begin{pmatrix} I_1^L & I_2^L & \cdots & I_M^L \end{pmatrix} = \begin{pmatrix} \hat{I}_1 & \hat{I}_2 & \hat{I}_3 \end{pmatrix} \begin{pmatrix} C_1 & C_1 & \cdots & C_M \end{pmatrix} \tag{5}$$

where $i_{(k,p)}^L = i_{(k,p)}$ at the pixel of diffuse reflection. In other words, $i_{(k,p)}^L = \mathbf{n}_p \cdot \mathbf{s}_k$ is satisfied in linearized images, and we can lead relationships such that a set of basis images $\mathbf{B} = \begin{pmatrix} \hat{I}_1 & \hat{I}_2 & \hat{I}_3 \end{pmatrix}$ and a set of coefficients $\mathbf{C} = \begin{pmatrix} C_1 & C_1 & \cdots & C_M \end{pmatrix}$can be represented as $\mathbf{B} = \begin{pmatrix} \mathbf{n}_1 & \mathbf{n}_2 & \cdots & \mathbf{n}_N \end{pmatrix}^T \cdot \Sigma$ and $\mathbf{C} = \Sigma^{-1} \cdot \begin{pmatrix} \mathbf{s}_1 & \mathbf{s}_2 & \cdots & \mathbf{s}_M \end{pmatrix}$ respectively, using the common 3×3 matrix Σ.

2.3 Classification using Linearized Images

As described above, each pixel of the input images can be classified into areas of diffuse reflection, specular reflection, attached shadow and cast shadow using the surface normal $\mathbf{n}$ and the lighting direction $\mathbf{s}$. Fortunately, we only use the product of these vectors $\mathbf{n} \cdot \mathbf{s}$, and we can also classify them by comparing the pixel values of the input and linearized images, $i_{(k,p)}$ and $i_{(k,p)}^L$ respectively. The classification does not need any additional information, such as 3D shapes, lighting directions, or color information.

In reality, captured images are affected by various types of noise. For example, imaging devices produce a dark current even if the intensity of the scene is zero. Also, the pixel intensity values are not perfectly linear

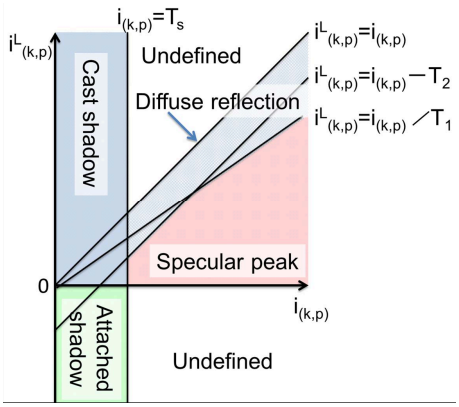

Figure 3: Criterion for photometric classification.

Figure 4: Specular lobe arise around specular peak.

in actual sensors, and so we often model these noises sources with additive and multiplicative noise models.

As shown in Figure 3, we classify each pixel with the following criteria.

$$\begin{cases} \text{Specular R.} & i_{(k,p)} > i_{(k,p)}^L * T_1 \cap i_{(k,p)} > i_{(k,p)}^L + T_2 \\ \text{Attached S.} & i_{(k,p)} < T_s \cap i_{(k,p)}^L \leq 0 \\ \text{Cast S.} & i_{(k,p)} < T_s \cap i_{(k,p)}^L > 0 \\ \text{Diffuse R.} & \textit{otherwise} \end{cases} \tag{6}$$

The thresholds T_1 and T_2 shown in Fig.3 are used to check the equality of $i_{(k,p)}$ and $i_{(k,p)}^L$ with certain multiplicative and additive noises. The threshold T_S is used to distinguish shadows. These thresholds can be determined through experiments with real images. In the linearization algorithm described below, we gradually decrease these thresholds to exclude the outliers properly.

2.4 Handling Specular Lobe

As mentioned in section2.1, the intensity observed at specular reflection points is greater than that at the points with diffuse reflection only. However, in reality, the difference is not always sufficiently large, and the thresholds T_1 and T_2 against noise will improperly include specular reflections to the inliers. More specifically, this phenomenon is commonly observed at specular lobes. As shown in Fig.4, specular lobes

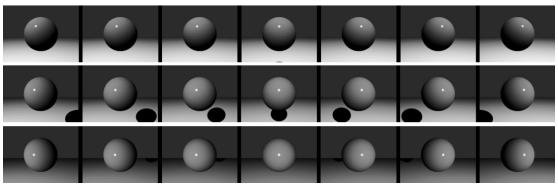

Figure 5: Input images.

surround the specular peaks, so we use spatial information to exclude such areas. While the linearization method using PCA described in the next section does not use the information about the neighboring relationships between pixels, we can exclude the erroneous area by increasing the area of the specular peaks by using the dilation operation. It is therefore important not only to exclude outliers during linearization, but also to use classification of optical phenomena to expand the specular reflection area only.

3 PHOTOMETRIC LINEARIZATION USING PCA

In this section, we present our linearization algorithm derived from principal component analysis (PCA). More specifically, we combine an outlier exclusion process based on the classification of photometric phenomena with repetitive PCA.

3.1 Algorithm

The following is the process for our linearization algorithm.

(A) Initialize.

For the photometric linearization, multiple images $\mathbf{I} = \begin{pmatrix} I_1 & I_2 & \cdots & I_M \end{pmatrix}$, $M > 3$ as shown in Fig.5 are taken using different lighting directions. While taking these images, the camera and the target objects should be fixed, and the information about the 3D shape, the lighting direction and the surface reflectance is not necessary. As an initialization, the input images are copied to the buffer of the inlier images, $\mathbf{I}^{IN} = \begin{pmatrix} I_1^{IN} & I_2^{IN} & \cdots & I_M^{IN} \end{pmatrix}$.

(B) Calculate Three Basis Images using PCA.

In the conventional method(Mukaigawa et al., 2007), three manually selected images are converted into linearized images using the RANSAC algorithm(Fischler and Bolles, 1981). However, as discussed earlier, this method has a problem in that the quality of the result depends heavily on the image selection. In contrast, we use all images to calculate the

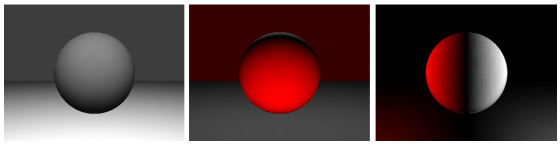

Figure 6: Three basis images (red color represents negative value).

Figure 7: Classification of photometric components.

linearized image using PCA. More specifically, we calculate the 1st, 2nd, and 3rd principal components $\mathbf{B} = \begin{pmatrix} \hat{I}_1 & \hat{I}_2 & \hat{I}_3 \end{pmatrix}$ of the matrix $\mathbf{I}^{IN}$ by analyzing the eigenvectors of the covariance matrix $\mathbf{I}^{IN}\mathbf{I}^{IN^T}$ without subtracting the mean of the input images. Because the principal components are orthogonal to each other, we can obtain linearly independent basis images as shown in Fig.6, where negative values are shown in red.

(C) Generate Linearized Images.

The coefficients of the linear combination $\mathbf{C}$ are determined by minimizing the root mean square errors between the input and linearized images as

$$\mathbf{C} = \mathbf{B}^T \mathbf{I}^{IN} \tag{7}$$

because $\mathbf{B}$ is the orthonormal basis and $\mathbf{B}^T\mathbf{B} = I$. The linearized images are then calculated by using the basis images and coefficients,

$$\mathbf{I}^L = \mathbf{B} \cdot \mathbf{C} \tag{8}$$

(D) Classification of Photometric Components.

As described in section 2.3, each pixel of each input image is classified into four photometric components, diffuse, specular peak, attached shadow and cast shadow, by comparing the pixel values of the input image $i_{(k,p)}$ and the linearized image $i^L_{(k,p)}$ based on the photometric classification criterion Eq.(6), as shown in Fig.3.

(E) Extension to Specular Lobe Area.

As shown in Fig.4, specular lobes arise around specular peaks. Therefore, pixels around the specular peak area are classified as outliers by the specular lobe. Fig.7 shows an example of classification for a scene with a sphere.

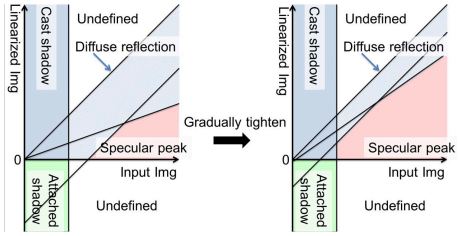

Figure 8: Tightening thresholds with each iteration.

(F) Pixel Value Replacement. Pixels affected by nonlinear illumination and reflection phenomena should be excluded as outliers for the next iteration of the PCA calculation,

$$\begin{cases} i^{IN}_{(k,p)} = i_{(k,p)} & \text{pixel of diffuse reflection} \\ i^{IN}_{(k,p)} = i^{L}_{(k,p)} & \text{pixel of specular reflection,} \\ & \text{specular lobe,} \\ & \text{attached and cast shadows} \end{cases} \quad (9)$$

(G) Tighten Thresholds and Iterate.

The algorithm starts from very loose thresholds to exclude the explicit outliers only. If such evident outliers are removed, the result of the next calculation becomes closer to the correct answer. Therefore, at this stage, thresholds T_1 and T_2 are slightly tightened towards the values determined for the sensor's noise level, as shown in Fig.8. Then, the process sequence from (B) to (G) is repeated until the thresholds reach the predetermined minimum values.

3.2 Example

Here, we show an example of each step of the linearization process for the input image shown in Fig.5. In Fig.9, ① shows one of the input images. Because the initial image contains nonlinear components, the linearized images calculated by step (C) contain artifacts, as shown in ② . By using the classification result shown in ③ , the pixel values at the outlier pixels of image ① are replaced by a linearized image ② in step (F), and the next input image ④ are generated. Here, the pixel intensities in the specular and cast shadow areas are relaxed, so the next linearized result ⑤ is better than the result calculated using the raw input images. The processes are repeated with tighter thresholds, and finally we obtain a clear linearized image ⑪ and correct classification results ⑫.

4 EXPERIMENTS

In this section, we show several experimental results.

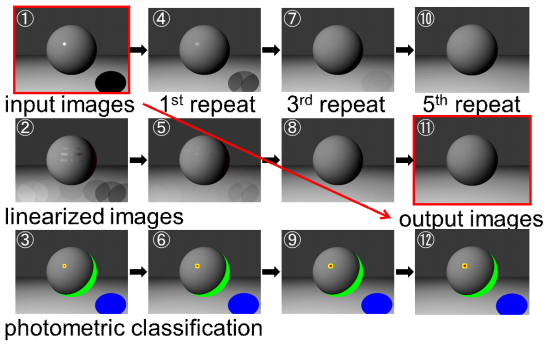

Figure 9: Example of the process of linearization by replacing outliers.

Computationally generated images are used for the quantitative evaluation because we can render the images without specular reflection and shadows as the ground truth. Results using real images show the robustness and feasibility of our method for the actual task.

4.1 Evaluation using Synthetic Images

First, we evaluated our proposed method by comparison with the conventional method(Mukaigawa et al., 2007) using synthetic images. The input images were generated by POV-Ray ray-tracing rendering software.

(A) Simple Convex Object.

The scene contains a sphere on a floor as shown in Fig.5. In some images, the cast shadow of the sphere is observed in the image on the floor. Twenty-one images were generated, using a different lighting direction for each image.

Fig.10(a) shows three manually selected images to be converted as basis images using the conventional method. As described above, the conventional method requires manual selection, which heavily affects the result. The selection shown in the figure is one of the adequate selections. Fig.10(b) shows the ground truths without specular reflection and shadows, corresponding to the three selected images. While we obtain linearized images for all input images in the final result, we will show these three images in the paper for comparison purposes.

The result of linearization by the conventional method are shown in Fig.10(c), with a corresponding error map (Fig.10(d)). Because the algorithm based on random sampling, the result shows some noise caused by the probabilistic fluctuation.

Unlike the conventional method, our algorithm does not require manual selection. Fig.10(e) shows the three basis images $\mathbf{B} = \begin{pmatrix} \hat{I}_1 & \hat{I}_2 & \hat{I}_3 \end{pmatrix}$ where the red

color indicates negative values. Using these basis images, we can linearize any input images. Fig.10(f) shows the results of the linearization of the three input images corresponding to the manually selected images for the conventional method. The colored error map shown in Fig.10(g) shows fewer errors when compared to that of the conventional method. A quantitative evaluation is shown in Table 1.

As described above, our method has the other advantage of fast calculation time. As shown in Table 2, our method is more than 100 times faster than the conventional method. This is because the conventional method uses the RANSAC(Fischler and Bolles, 1981) algorithm to remove the non-Lambertian components and runs an enormous number of iterative calculations. If the number of iterations is limited, the result is degraded.

Table 1: Quantitative evaluation of the result.

	Mean error	Variance	Max. error
Conventional	2.420	2.688	22
Proposed	0.831	1.933	16

Table 2: Comparison of the calculation time.

	Calculation time[s]
Conventional	3.930×10^3
Proposed	1.424×10^1

Fig.10(h) shows the classification results using the proposed method. In this figure, the red, yellow, green and blue pixels correspond to the specular peaks, specular lobes, attached shadows and cast shadows respectively. It is evident that the classification has been performed correctly.

(B) Complex Shaped Object.

We then show the results for the complex shaped object. The object shape is that of a Stanford bunny, as shown in Fig.11. Twenty-five images were generated, using a different lighting direction for each image.

In Fig.12, we show the results of the conventional and proposed methods in the same order as Fig.10. In this case, the conventional method fails. Fig.12(c) shows that the results contain the remaining specular areas and noisy values, and the error map shown in Fig.12(d) also indicates erroneous results. In contrast, the proposed method offers adequate results, as shown in Fig.12(f), which are close in appearance to the ground truths shown in Fig.12(b). The error map shown in Fig.12(g) also shows fewer noise compared to that of the conventional method. Table 3 also indicates a clear difference between the conventional and

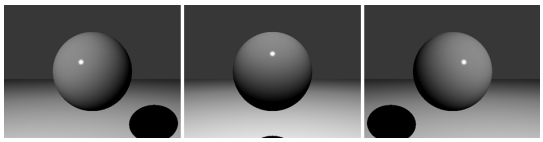

(a) Images to be linearized by conventional method.

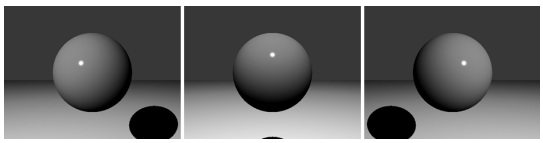

(b) Ground truths.

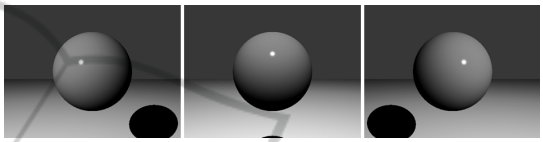

(c) Linearized by conventional method.

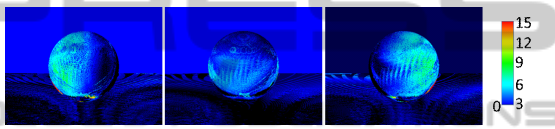

(d) Error map of conventional method.

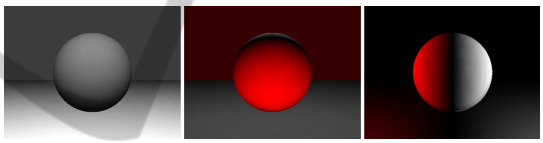

(e) Three basis images generated by proposed method.

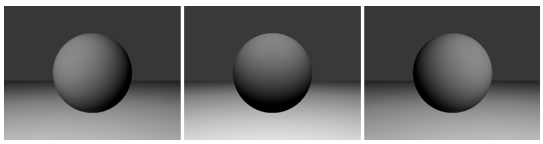

(f) Linearized by proposed method.

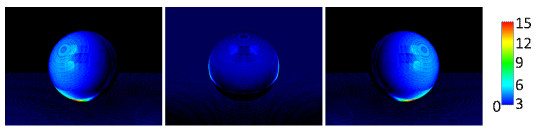

(g) Error map of proposed method.

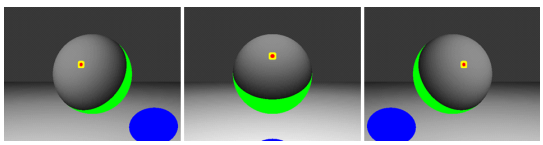

(h) Classified by proposed method.

Figure 10: Linearization of synthetic convex object.

proposed methods. The classification results from our method shown in Fig.12(h) also show that our results are correct. The calculation time shown in Table4 shows similar differences to the case of the sphere scene.

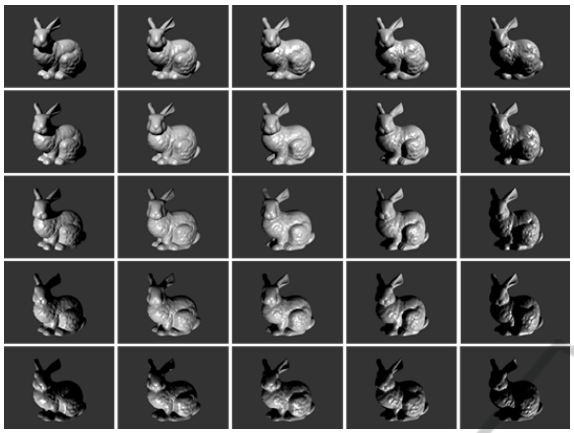

Figure 11: Input images.

Table 3: Numerical evaluation of the linearization result.

	Mean error	Variance	Max. error
Conventional	9.634	410.740	255
Proposed	3.716	28.107	151

Table 4: Comparison of the calculation time.

	Calculation time[s]
Conventional	5.132×10^3
Proposed	1.488×10^1

4.2 Evaluation using Real Images

In this section we use real images taken with a camera. The scene contains a pot, as shown in Fig.13. Twenty-four images were captured, using a different lighting direction for each one.

Fig.14(a) shows the three input images selected for linearization by the conventional method. Fig.14(c) shows the linearization result generated by the conventional method, while Fig.14(d) shows the linearization result generated by the proposed method. Both results are similar, but, we can see some noisy fluctuations on the results from the conventional method. In contrast, the proposed method provides smooth images without specular reflections. Figure 14(e) shows that our algorithm properly classifies the phenomena observed on the object. The proposed method also has the advantage of being much faster than the conventional method as shown in Table5.

Table 5: Comparison of the calculation time.

	Calculation time[s]
Conventional	8.028×10^3
Proposed	1.675×10^1

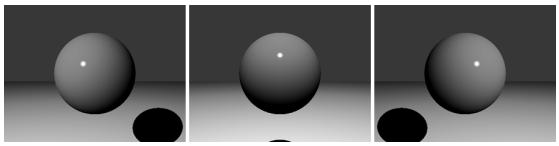

(a) Images to be linearized by conventional method.

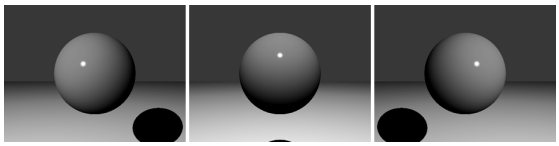

(b) Ground truth.

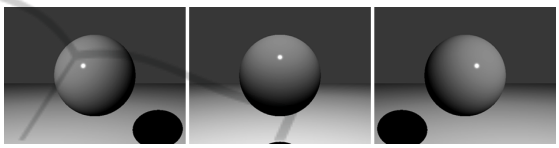

(c) Linearized by conventional method.

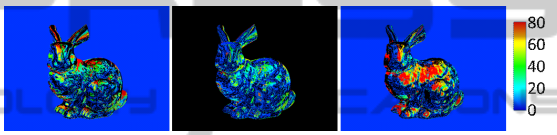

(d) Error map of conventional method.

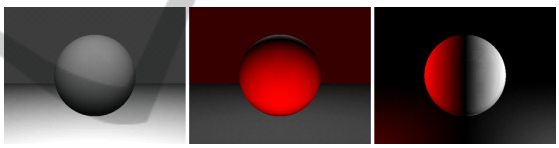

(e) Three basis images generated by proposed method.

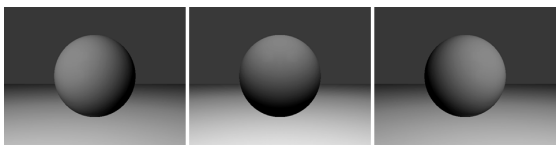

(f) Linearized by proposed method.

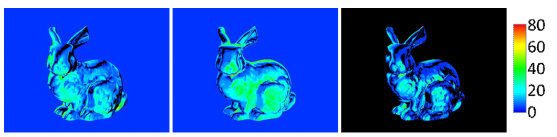

(g) Error map of proposed method.

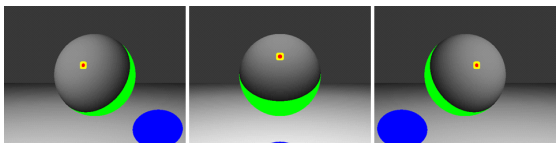

(h) Classified by proposed method.

Figure 12: Linearization of complex shaped object.

Figure 13: Input images.

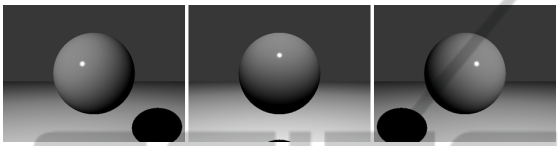

(a) Images to be linearized by conventional method.

(b) Three basis images generated by proposed method.

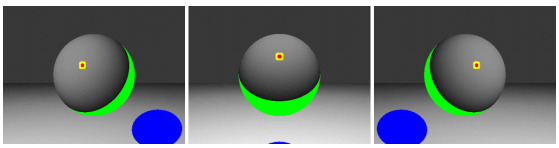

(c) Linearized by conventional method.

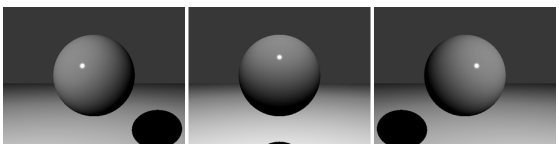

(d) Linearized by proposed method.

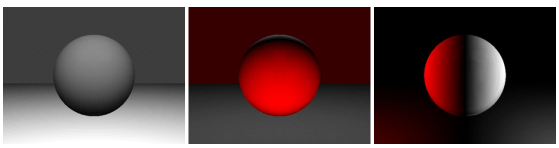

(e) Classified by proposed method.

Figure 14: Linearization of real images.

5 CONCLUSIONS

We focused on the approach of the conventional photometric linearization method(Mukaigawa et al., 2007), which selects three basis images from real images, including not only diffuse reflections but also specular reflections and shadows. The conversion accuracy thus becomes unstable and is seriously influenced by the selection of the three basis images, and it also takes a long time to remove the non-Lambertian components, e.g. the specular reflections and shadows. We therefore proposed a novel pixel value replacement algorithm using photometric classification, which enables us to uniquely generate three ideal basis images, including only diffuse reflections from real images, and enables us to generate accurate ideal images stably and quickly. We then confirmed the effectiveness of the proposed method experimentally.

ACKNOWLEDGEMENTS

The authors are grateful to Prof. Mukaigawa and Mr. Ishii for providing their source codes and real images presented in their paper (Mukaigawa et al,, 2007) for our comparisons shown in Section 4. This work was partially supported by Grant-in-Aid for Scientific Research (B:21300067) and Grant-in-Aid for Scientific Research on Innovative Areas (22135003).

REFERENCES

Belhumeur, P. and Kriegman, D. (1996). What is the set of images of an object under all possible lighting conditions? In *cvpr*, page 270. Published by the IEEE Computer Society.

Fischler, M. and Bolles, R. (1981). Random sample consensus: a paradigm for model fitting with applications to image analysis and automated cartography. *Communications of the ACM*, 24(6):381–395.

Georghiades, A., Belhumeur, P., and Kriegman, D. (2001). From few to many: Illumination cone models for face recognition under variable lighting and pose. *Pattern Analysis and Machine Intelligence, IEEE Transactions on*, 23(6):643–660.

Ikeuchi, K. and Sato, K. (1991). Determining reflectance properties of an object using range and brightness images. *IEEE Transactions on Pattern Analysis and Machine Intelligence*, pages 1139–1153.

Klinker, G., Shafer, S., and Kanade, T. (1988). The measurement of highlights in color images. *International Journal of Computer Vision*, 2(1):7–32.

Mukaigawa, Y., Ishii, Y., and Shakunaga, T. (2007). Analysis of photometric factors based on photometric linearization. *JOSA A*, 24(10):3326–3334.

Mukaigawa, Y., Miyaki, H., Mihashi, S., and Shakunaga, T. (2001). Photometric image-based rendering for image generation in arbitrary illumination. In *Computer Vision, 2001. ICCV 2001. Proceedings. Eighth IEEE International Conference on*, volume 2, pages 652–659. IEEE.

Nayar, S., Fang, X., and Boult, T. (1993). Removal of specularities using color and polarization. In *Computer Vision and Pattern Recognition, 1993. Proceedings CVPR'93., 1993 IEEE Computer Society Conference on*, pages 583–590. IEEE.

Sato, Y. and Ikeuchi, K. (1994). Temporal-color space analysis of reflection. *JOSA A*, 11(11):2990–3002.

Sato, Y., Wheeler, M., and Ikeuchi, K. (1997). Object shape and reflectance modeling from observation. In *Proceedings of the 24th annual conference on Computer graphics and interactive techniques*, pages 379–387. ACM Press/Addison-Wesley Publishing Co.

Shafer, S. (1985). Using color to separate reflection components from a color image. *Color Research and Applications*, 10(4):210–218.

Shashua, A. (1992). *Geometry and photometry in 3D visual recognition*. PhD thesis, Citeseer.

Wolff, L. and Boult, T. (1991). Constraining object features using a polarisation reflectance model. *IEEE Trans. Patt. Anal. Mach. Intell*, 13:635–657.